OTC 19458

Numerical Simulation of Methane Hydrate Production from Geologic Formations via Carbon Dioxide Injection

M.D. White, Pacific Northwest National Laboratory; B.P. McGrail, SPE, Pacific Northwest National Laboratory

This paper was prepared for presentation at the 2008 Offshore Technology Conference held in Houston, Texas, U.S.A., 5–8 May 2008.

Abstract

Scientific and technological innovations are needed to realize effective production of natural gas hydrates. Whereas global estimates of natural gas hydrate reservoirs are vast, accumulations vary greatly in nature and form. Suboceanic deposits vary from disperse concentrations residing at low saturations in the pore space of unconsolidated sediments with sand-sized particles to higher concentrations residing in the fractures of sediments with clay-sized particles. Conventional methods for gas hydrate production include depressurization, thermal stimulation, and inhibitor injection. For suboceanic accumulations in sandy sediments, depressurization has been shown, through numerical simulation, to be the most feasible production technology. However, recovery efficiencies are too low to justify pursuing these energy reservoirs. Under high pressure, low temperature suboceanic conditions the hydrate structure can accommodate small molecules other than methane (CH_4), such as carbon dioxide (CO_2) and nitrogen (N_2) in both the small and large cages. Although CO_2 and N_2 clathrates generally are not naturally as abundant as those of CH_4, their occurrence forms the foundation of an unconventional approach for producing natural gas hydrates that involves the exchange of CO_2 with CH_4 in the hydrate structure. This unconventional concept has several distinct benefits over the conventional methods: 1) the heat of formation of CO_2 hydrate is greater than the heat of dissociation of CH_4 hydrate, providing a low-grade heat source to support additional methane hydrate dissociation, 2) exchanging CO_2 with CH_4 will maintain the mechanical stability of the geologic formation, and 3) the process is environmentally friendly, providing a sequestration mechanism for the injected CO_2. An operational mode of the STOMP simulator has been developed at the Pacific Northwest National Laboratory that solves the coupled flow and transport equations for the mixed CH_4-CO_2 hydrate system under nonisothermal conditions, with the option for considering NaCl as an inhibitor in the pore water. This paper describes the numerical simulator, its formulation, assumptions, and solution approach and demonstrates, via numerical simulation, the production of gas hydrates from permafrost accumulations in sandstone formations with high gas hydrate saturations and suboceanic accumulations in sandy sediments with low hydrate saturations using the CO_2-CH_4 exchange technology.

Introduction

Gas hydrates are clathrate compounds in which water molecules encapsulate a guest molecule within a lattice structure. The lattice structure of gas hydrates form under low temperature, high pressure conditions via hydrogen bonding between water molecules. Gas hydrates with methane (CH_4) guest molecules are abundant as geologic accumulations in offshore and permafrost environments where sufficiently low temperature and high pressure conditions exist. From an energy resource perspective, these geologic accumulations of natural gas hydrates represent a significant component of the world's organic carbon sources. Recent surveys by the United States Geological Survey (USGS) have estimated that reserves of methane in hydrate form exceed the all other fossil fuel forms of organic carbon (Booth et al., 1996). Under geologic environmental conditions, the lattice structure of a gas hydrate depends primarily on the guest molecule (Englezos, 1993; and Sloan, 1998). Interestingly, the two most prevalent emitted greenhouse gases (U.S. EPA, 2006) carbon dioxide (CO_2) and methane (CH_4) both form sI hydrate structures under geologic temperature and pressure conditions. Whereas their clathrate structures are similar, CO_2 hydrates form at higher temperatures and have a higher enthalpy of formation compared with CH_4 hydrates (Sloan, 1998).

Natural gas can be produced from geologic accumulations of natural gas hydrates either by dissociating the clathrate structure, yielding liquid water and gaseous methane, or by replacing the CH_4 molecule with another guest. Conventional

approaches to producing natural gas hydrate are through clathrate dissociation: 1) thermal stimulation, 2) depressurization, and 3) inhibitor injection. The thermal stimulation approach involves raising the hydrate temperature above the stability point, causing the hydrate to dissociate. Thermal stimulation requires a continuous energy source to overcome the endothermic heat of dissociation. Depressurization involves lowering the hydrate pressure below the stability point, causing the hydrate to dissociate. Depressurization results in rapid hydrate dissociation, but with an associate drop in the hydrate temperature. Without an external heat source, depressurization lowers the hydrate temperature to a new equilibrium condition, halting the depressurization process. Inhibitor injection involves the injection of an organic or inorganic compound that shifts the hydrate equilibrium point to lower temperatures for isobaric conditions. As with depressurization, inhibitor injection could require additional inhibitor or a heat source to compensate for the decrease in hydrate temperature with dissociation.

The concept of exchanging CO_2 with CH_4 as guest molecules in geologic accumulations of natural gas hydrates as a production technology was first advanced by Ohgaki et al. (1996). This concept was then extended to ethane hydrates by Nakano et al. (1998). Their original concept involved injecting CO_2 gas into an aqueous-gas-hydrate system and allowing the CO_2 and CH_4 to equilibrate. The greater chemical affinity for CO_2 over CH_4 in the hydrate structure, as evidenced by the higher heat of formation and equilibrium temperature, yields a mixed CO_2-CH_4 hydrate. Resulting equilibrium concentrations of CO_2 are greater than CH_4 in the hydrate phase and less than CH_4 in the gas phase. If this molecular exchange technology can be realized for field production of geologic accumulations of natural gas hydrates, it could offer two secondary benefits; mechanical stability and mitigating global warming. If the exchange process is conducted without significant hydrate dissociation the mechanical stability of the hydrate-bearing formation could be maintained. The exchange technology would additionally represent a nearly neutral carbon process, sequestering one molecule of CO_2 for each produced molecule of CH_4, which could then be burned to produce energy and CO_2.

Since the original studies by Ohgaki et al. (1996), Hirohama et al. (1996), and Komai et al. (1997), the CO_2-CH_4 exchange technology has been investigated by others. Smith et al. (2001) assessed the feasibility of exchanging CO_2 with CH_4 in geologic accumulations of gas hydrate by examining the thermodynamic potential for the exchange as a function of pore sizes. This study concluded that the replacement of CH_4 by CO_2 in geologic accumulations of gas hydrate is less thermodynamically favored as pore size decreases. Rice (2003; 2006) has proposed a methane hydrate production scheme for suboceanic deposits that yields hydrogen and carbon dioxide. In this scheme methane hydrate is produced using conventional technologies (e.g., thermal stimulation, depressurization) and the captured CO_2 is sequestered on the ocean floor or in the suboceanic sediments in hydrate form. Whereas Rice's scheme involves CO_2 sequestration in hydrate form, the CO_2-CH_4 molecular exchange is indirect, requiring hydrate dissociation and subsequent reformation. McGrail et al. (2004) proposed a concept for exchanging CO_2 with CH_4 in geologic deposits of gas hydrate by injecting a microemulsion of liquid CO_2 and water. The microemulsion is designed to provide sensible heat to dissociate the CH4 hydrate, taking advantage of the higher heat of formation for the CO_2 hydrate versus the CH_4 hydrate. This technology was demonstrated in laboratory columns and numerically simulated (White and McGrail, 2006). Castaldi et al. (2007) investigated the technical feasibility of a down-hole combustion method for producing natural gas hydrate and sequestering CO_2. The details of replacing CO_2 with CH_4 in the hydrate structure was left unspecified, other than requiring a balance in the rates of CH_4 hydrate dissociation and CO_2 hydrate formation. The thermodynamics of this approach are favorable, but the implementation remains a technical challenge.

This paper investigates, using numerical simulation, the production of natural gas hydrates from geologic deposits via the combined processes of depressurization, thermal stimulation and direct molecular exchange of CO_2 and CH_4. Numerical simulations are conducted using a five-spot well configuration with the center well being an extraction or injection well and perimeter wells being strictly extraction wells. During the injection stages CO_2 is injected as either liquid, subcritical gas, or supercritical gas. Liquid-CO_2 is assumed to form a separate phase from the aqueous and gas phases, having an intermediate wettability between the aqueous and gas phases. Two implementations of the numerical simulator are described: 1) equilibrium and 2) kinetic. In the equilibrium implementation the CO_2 and CH_4 components (i.e., hydrate forming components) in the mobile phases (i.e., aqueous, liquid-CO_2, and gas) are assumed to be in equilibrium with their counterparts in the immobile phase (i.e., hydrate). In the kinetic implementation the CO_2 and CH_4 components in the mobile and immobile phases are tracked separately, with a kinetic rate controlling the exchange of hydrate forming components between the mobile and immobile phases. In both implementations the water component is assumed to be in equilibrium between the mobile and immobile phases. The objective of these numerical investigations is to demonstrate the feasibility of directly injecting CO_2 into a natural gas hydrate bearing reservoir to produce CH_4, where the principal concerns are production rates and energy costs.

Mathematical Model

The mathematical model for both the equilibrium and kinetic implementations of the numerical simulator comprise governing conservation equations and associated constitutive equations that relate the primary unknowns with the secondary variables. The equilibrium implementation, referred to as STOMP-HYD, solves the conservation equations for water mass,

CH_4 mass, CO_2 mass, inhibitor mass, and energy with an option for solving an inhibitor mass equation. The kinetic implementation, referred to as STOMP-HYD-KNC, divides the conservation of hydrate formers mass (i.e., CH_4 and CO_2 mass) into mobile phase (i.e., aqueous, liquid-CO_2, and gas) and immobile phase (i.e., hydrate) components. The conservation equations equate the change in the conserved quantity within a volume over time with the net flux of the conserved quantity into the volume plus any net source of the conserved quantity with the volume. The conservation equation for energy is identical for both the equilibrium and kinetic implementations;

$$\frac{\partial}{\partial t}\left[\sum_{\gamma=l,n,g,h,i,p}\left(\phi_D\,\rho_\gamma\,s_\gamma\,u_\gamma\right)+(1-\phi_T)\,\rho_s\,u_s+(\phi_T-\phi_D)\,\rho_l\,u_l\right]= \\ -\sum_{\gamma=l,n,g}\nabla\left(\rho_\gamma\,h_\gamma\,\mathbf{V}_\gamma\right)-\sum_{i=w,a,o}\nabla\left(h_g^i\,\mathbf{J}_g^i\right)+\nabla\left(\mathbf{k}_e\,\nabla\,T\right)+\sum_{\gamma=l,n,g}\left(h_\gamma\,m_\gamma\right)+q\ . \tag{1}$$

Advective fluxes of the mobile phases are computed according to Darcy's law;

$$\mathbf{V}_\gamma=-\frac{k_{r\gamma}\,\mathbf{k}}{\mu_\gamma}\left(\nabla\,P_\gamma+\rho_\gamma\,g\,\mathbf{z}_g\right)\ . \tag{2}$$

Diffusive/dispersive fluxes of the components through the mobile phases are computed from gradients in molar concentration, considering both molecular diffusion and hydraulic dispersion;

$$\mathbf{J}_\gamma^i=-\phi_D\,\rho_\gamma\,s_\gamma\,\frac{M^i}{M_\gamma}\left(\tau_\gamma\,D_\gamma^i+\mathbf{D}_{h_\gamma}\right)\nabla\,\chi_\gamma^i\ . \tag{3}$$

For the equilibrium implementation the conservation of component mass includes both mobile and immobile phases;

$$\frac{\partial}{\partial t}\left[\sum_{\gamma=l,n,g,h,i,p}\left(\phi_D\,\omega_\gamma^i\,\rho_\gamma\,s_\gamma\right)\right]=-\sum_{\gamma=l,n,g}\nabla\left(\omega_\gamma^i\,\rho_\gamma\,\mathbf{V}_\gamma\right) \\ -\sum_{\gamma=l,n,g}\nabla\left(\mathbf{J}_\gamma^i\right)+\sum_{\gamma=l,n,g}\omega_\gamma^i\,m_\gamma\quad for\ i=w,a,o\ . \tag{4}$$

For the kinetic implementation the conservation equations for mobile CO_2 and CH_4 component masses include a kinetic rate term for exchange between the mobile phases and hydrate phase;

$$\frac{\partial}{\partial t}\left[\sum_{\gamma=l,n,g}\left(\phi_D\,\omega_\gamma^i\,\rho_\gamma\,s_\gamma\right)\right]=-\sum_{\gamma=l,n,g}\nabla\left(\omega_\gamma^i\,\rho_\gamma\,\mathbf{V}_\gamma\right) \\ -\sum_{\gamma=l,n,g}\nabla\left(\mathbf{J}_\gamma^i\right)+\sum_{\gamma=l,n,g}\omega_\gamma^i\,m_\gamma-K_h\left(P_g^i-\varphi_g^i\,P_h^{eq}\right)\quad for\ i=a,o\ . \tag{5}$$

The conservation equations for the hydrate CO_2 and CH_4 component mass relate the kinetic exchange of components between the mobile phases and hydrate to the change in hydrate component mass;

$$\frac{\partial}{\partial t}\left(\phi_D\,\omega_h^i\,\rho_h\,s_h\right)=K_h\left(P_g^i-\varphi_g^i\,P_h^{eq}\right)\quad for\ i=a,o\ . \tag{6}$$

The governing conservation equations were solved with integral volume differencing on structured orthogonal grids, using Newton-Raphson iteration to resolve the nonlinearities. Details of the numerical solution scheme for STOMP are described in the simulator theory guide (White and Oostrom, 2000).

The numerical simulations conducted for this paper ignored the formation salinity; therefore, the inhibitor mass conservation equation was not included in the solved equations. The equilibrium implementation had four conservation equations and primary unknowns for each grid cell, and the kinetic implementation solved two additional equations for two additional primary unknowns. Primary unknowns for the conservation equations are chosen to be independent and able to completely define the system state, which implies being able to compute the suite of secondary variables. With the possibility for phase appearances and disappearances, there does not exist a single set of primary variables that can be used to define the system state for every phase condition possibility. To overcome this numerical difficulty, a primary variable switching scheme was developed that changes the primary variable set with phase conditions. To ensure smooth transitions across phases, the primary variable switching occurs between Newton-Raphson iterations within a single time step. Two different primary variable switching schemes were developed for the equilibrium and kinetic implementations.

There are four primary variable sets for the equilibrium implementation, as shown in Table 1, distinguished by the appearance and disappearance of the hydrate and liquid-CO_2 phases. Transitions from no-hydrate to hydrate conditions occur when the temperature drops below the hydrate equilibrium temperature. Transitions from no-liquid-CO_2 to liquid-CO_2

conditions occur when the vapor partial pressure of CO_2 exceeds the saturated liquid-CO_2 vapor pressure. In Phase Condition #4, resolution of the hydrate equilibrium pressure, gas mole fraction of hydrate formers, and CH_4 vapor pressure is solved via Newton-Raphson iteration. There are two primary variable sets for the kinetic implementation, as shown in Table 2, distinguished by the appearance and disappearance of the liquid-CO_2 phase. The additional primary variables of the kinetic implementation eliminate two phase conditions, but at the computational cost of two additional unknowns per grid cell. As with the equilibrium implementation, transitions from no-liquid-CO_2 to liquid-CO_2 conditions occur when the vapor partial pressure of CO_2 exceeds the saturated liquid-CO_2 vapor pressure.

Table 1 – Equilibrium Primary Variable Sets

Phase Condition #1 (no hydrate, no liquid CO_2) - $s_l \le 1,\ s_g \ge 0,\ s_n = 0,\ s_h = 0,\ s_i \ge 0$			
Energy - T	H_2O Mass - P_l	CH_4 Mass - $P_g^{CH_4}$	CO_2 Mass - $P_g^{CO_2}$
$P_g = \max\left[\left(P_l + \frac{\beta_{gl}}{\psi}\right), \left(P_g^{CO_2} + P_g^{CH_4} + P_g^{H_2O}\right)\right],\ P_n = P_n^c,$			
$P_h^{eq} = P_g^{CO_2} + P_g^{CH_4},\ T_h^{eq} = func\left[P_h^{eq}, \varphi_g^{CH_4}\right]$			
Phase Condition #2 (hydrate, no liquid CO_2) - $s_l \le 1,\ s_g \ge 0,\ s_n = 0,\ s_h > 0,\ s_i \ge 0$			
Energy - T	H_2O Mass - P_l	CH_4 Mass - s_h	CO_2 Mass - $\varphi_g^{CH_4}$
$P_g = \max\left[\left(P_l + \frac{\beta_{gl}}{\psi}\right), \left(P_g^{CO_2} + P_g^{CH_4} + P_g^{H_2O}\right)\right],\ P_n = P_n^c,$			
$P_h^{eq} = func\left[T, \varphi_g^{CH_4}\right],\ P_g^{CH_4} = P_h^{eq}\,\varphi_g^{CH_4},\ P_g^{CO_2} = P_h^{eq} - P_g^{CH_4}$			
Phase Condition #3 (no hydrate, liquid CO_2) - $s_l \le 1,\ s_g \ge 0,\ s_n > 0,\ s_h = 0,\ s_i \ge 0$			
Energy - T	H_2O Mass - P_l	CH_4 Mass - $P_g^{CH_4}$	CO_2 Mass - P_n
$P_g = \max\left[\left(P_l + \frac{\beta_{gl}}{\psi}\right), \left(P_g^{CO_2} + P_g^{CH_4} + P_g^{H_2O}\right)\right],\ P_g^{CO_2} = P_{sat}^{CO_2},$			
$P_h^{eq} = P_g^{CO_2} + P_g^{CH_4},\ T_h^{eq} = func\left[P_h^{eq}, \varphi_g^{CH_4}\right]$			
Phase Condition #4 (hydrate, liquid CO_2) - $s_l \le 1,\ s_g \ge 0,\ s_n > 0,\ s_h > 0,\ s_i \ge 0$			
Energy - T	H_2O Mass - P_l	CH_4 Mass - s_h	CO_2 Mass - P_n
$P_g = \max\left[\left(P_l + \frac{\beta_{gl}}{\psi}\right), \left(P_g^{CO_2} + P_g^{CH_4} + P_g^{H_2O}\right)\right],\ P_g^{CO_2} = P_{sat}^{CO_2},$			
$P_h^{eq} = func\left[T, \varphi_g^{CH_4}\right],\ P_g^{CH_4} = P_h^{eq}\,\varphi_g^{CH_4},\ \varphi_g^{CH_4} = P_g^{CH_4} / \left(P_g^{CH_4} + P_g^{CO_2}\right)$			

The constitutive equations relate the secondary variables to the primary variables. In general, these equations are nonlinear. The STOMP-HYD and -HYD-KNC simulators include constitutive equations that are both general to all operational modes of the STOMP simulator and specific to the hydrate operational modes and implementations. Those constitutive equations general to all operational modes of the STOMP simulator are documented in the STOMP Theory Guide (White and Oostrom, 2000). Those constitutive equations specific to the hydrate operational mode will be briefly described. The properties of CO_2 (e.g., density, viscosity, internal energy, enthalpy, thermal conductivity) are computed using tabulated data generated from the Span and Wagner (1996) formulations. The properties of CH_4 (e.g., density, viscosity, internal energy, enthalpy, thermal conductivity) are computed using tabulated data generated from the Setzmann and Wagner (1991) formulations. The equilibrium pressure and temperature relationships for mixed hydrates are computed using tabulated data generated from the Klauda and Sandler (2003) formulations. The hydrate properties (e.g., density, enthalpy, cage occupancies) for mixed

hydrates are computed from the formulations of Sloan (1998). Changes to the equilibrium pressure and temperature relationships with respect to inhibitor concentrations are computed using tabular data and formulations published by Heriot-Watt Institute of Petroleum Engineering (Østergaard et al., 2005).

Table 2 – Kinetic Primary Variable Sets

Phase Condition #1 (no liquid CO_2) - $s_l \le 1$, $s_g \ge 0$, $s_n = 0$, $s_h \ge 0$, $s_i \ge 0$					
Energy - T	H_2O Mass - P_l	Mobile CH_4 Mass - $P_g^{CH_4}$	Mobile CO_2 Mass - $P_g^{CO_2}$	Hydrate CH_4 Mass - $P_{h_{eq}}^{CH_4}$	Hydrate CO_2 Mass - $P_{h_{eq}}^{CO_2}$
$P_g = \max\left[\left(P_l + \frac{\beta_{gl}}{\psi}\right), \left(P_g^{CO_2} + P_g^{CH_4} + P_g^{H_2O}\right)\right]$, $P_n = P_n^c$, $P_h^{eq} = P_{h_{eq}}^{CO_2} + P_{h_{eq}}^{CH_4}$, $T_h^{eq} = func\left[P_h^{eq}, \varphi_g^{CH_4}\right]$					
Phase Condition #2 (liquid CO_2) - $s_l \le 1$, $s_g \ge 0$, $s_n > 0$, $s_h \ge 0$, $s_i \ge 0$					
Energy - T	H_2O Mass - P_l	Mobile CH_4 Mass - $P_g^{CH_4}$	Mobile CO_2 Mass - P_n	Hydrate CH_4 Mass - $P_{h_{eq}}^{CH_4}$	Hydrate CO_2 Mass - $P_{h_{eq}}^{CO_2}$
$P_g = \max\left[\left(P_l + \frac{\beta_{gl}}{\psi}\right), \left(P_g^{CO_2} + P_g^{CH_4} + P_g^{H_2O}\right)\right]$, $P_g^{CO_2} = P_{sat}^{CO_2}$, $P_h^{eq} = P_{h_{eq}}^{CO_2} + P_{h_{eq}}^{CH_4}$, $T_h^{eq} = func\left[P_h^{eq}, \varphi_g^{CH_4}\right]$					

Relationships between phase pressures and phase saturations, and phase saturations and phase relative permeabilities are additionally required to compute the transport properties of the system. In the subject version of the simulator, hydrate saturation is assumed to be independent of pore radii and capillary pressure. In previous versions of the simulator (White and McGrail, 2006) hydrate was assumed to be totally occluded by the aqueous phase and the hydrate saturation was computed as a function of the pore-size distribution and the difference between the temperature and bulk equilibrium temperature for the hydrate. For no-liquid-CO_2 conditions the aqueous saturation is a function of the capillary pressure between the gas and aqueous phases and the hydrate and ice saturations,

$$\bar{\bar{s}}_l = \frac{\frac{s_l}{\left(1 - s_h - s_i\right)} - s_{lr}}{\left(1 - s_{lr}\right)} = func\left[\beta_{gl}\left(P_g - P_l\right)\right]; \text{ where } \beta_{gl} = \frac{\sigma_{ref}}{\sigma_{gl}}. \tag{7}$$

This approach assumes that the form of the moisture retention characteristic curve is maintained as the immobile hydrate and ice phases fill the pore space. Moreover, for no-liquid-CO_2 conditions, the liquid-CO_2 pressure is set to the critical phase pressure

$$P_n = \frac{\beta_{nl}\ P_l + \beta_{gn}\ P_g}{\beta_{nl} + \beta_{gn}}; \text{ where } \beta_{gn} = \frac{\sigma_{ref}}{\sigma_{gn}}. \tag{8}$$

For liquid-CO_2 conditions the aqueous saturation is a function of the capillary pressure between the liquid-CO_2 and the aqueous pressure

$$\bar{\bar{s}}_l = \frac{\frac{s_l}{\left(1 - s_h - s_i\right)} - s_{lr}}{\left(1 - s_{lr}\right)} = func\left[\beta_{nl}\left(P_n - P_l\right)\right]; \text{ where } \beta_{nl} = \frac{\sigma_{ref}}{\sigma_{nl}}. \tag{9}$$

The liquid-CO_2 saturation is computed indirectly from the total-liquid (i.e., aqueous + liquid CO_2) saturations; where the total-liquid saturation is a function of the capillary pressure between the gas and liquid-CO_2 phases

$$s_n = s_t - s_l; \text{ where } \bar{\bar{s}}_t = \frac{\frac{s_t}{\left(1 - s_h - s_i\right)} - s_{lr}}{\left(1 - s_{lr}\right)} = func\left[\beta_{gn}\left(P_g - P_n\right)\right]. \tag{10}$$

Permeabilities are required for the three mobile phases (i.e., gas, liquid-CO_2, and aqueous). Phase permeabilities are computed as the product of the intrinsic permeability and the phase relative permeability. There are two conventional approaches to addressing the impact of the immobile phases (i.e., hydrate and ice) on the phase permeabilities: 1) variable intrinsic permeability, and 2) constant intrinsic permeability. In the variable intrinsic permeability approach the immobile phases are considered to alter the intrinsic permeability of the geologic media via the Kozeny-Carman equation (McCabe et al., 2005) or alterative function. The phase relative permeability is then computed as a function of the effective phase saturations. In the constant intrinsic permeability approach, the intrinsic permeability is considered a constant, and the phase relative permeabilities are computed using effective phase saturations defined from the actual saturations

$$k_{rg} = func\left[\frac{s_t - s_{lr}}{1 - s_{lr}}\right]; k_{rn} = func\left[\frac{s_t - s_{lr}}{1 - s_{lr}}, \frac{s_l - s_{lr}}{1 - s_{lr}}\right]; k_{rl} = func\left[\frac{s_l - s_{lr}}{1 - s_{lr}}\right]. \quad (11)$$

In the constant intrinsic permeability approach, the effect of the immobile phases is incorporated indirectly through the use of the actual phase saturations. The constant intrinsic permeability approach was applied for the simulations reported in this paper.

Numerical Simulations

The CO_2-CH_4 molecular exchange process is driven by the lower energy state of CO_2 as the guest molecule in sI gas hydrate structures versus CH_4. This results in higher equilibrium temperatures and heats of formation for the pure CO_2 versus pure CH_4 hydrates. These favorable thermodynamics for CO_2 versus CH_4 hydrates can be used advantageously to produce natural gas hydrates, but also have a disadvantage for geologic environments in that secondary mixed hydrates can form, clogging the pore space and halting production. To investigate these competing processes for the production of a natural gas hydrate reservoir using CO_2 injection and depressurization, a series of simulations were conducted on an idealized five-spot well system. The computational domain modeled ¼ of a 1-m thick five-spot well system with outer well spacings of 100 m. Two types of geologic accumulations were considered: 1) sandstone formations beneath the permafrost with high hydrate saturations, and 2) suboceanic sandy sediments with low hydrate saturations. Simulations and results for the permafrost environment are described in this paper. Simulations and results for the suboceanic environment will be presented during with the presentation of this paper.

The geologic media was assumed to be a sandstone with intrinsic permeability of 1 Darcy, porosity of 0.35, and compressibility of 6.25e-10 1/Pa. The capillary pressure-saturation relationships were defined via the van Genuchten function (van Genuchten, 1980) with α = 10.204 1/m, n = 4.432, and s_{lr} = 0.1. The phase relative permeability relations were defined by the Mualem functions (Mualem, 1976). For the effective thermal conductivity, a volume averaging model was applied with a grain conductivity of 2.0 W/m K and a grain specific heat of 700 J/kg. Zero reservoir salinity was assumed.

Initially the hydrate reservoir was assumed to be at 6 MPa and 3 C with a pure CH_4 hydrate of 0.7 saturation. The gas-aqueous, liquid CO_2-aqueous, hydrate-aqueous, and reference interfacial tensions were set to 72.0, 24.0, 26.7, and 72.0 dynes/cm, respectively. Injection and production wells were modeled using surface boundary conditions. Aside from the surface boundaries, representing the injection and production wells, all other boundaries were assigned no flow (i.e., adiabatic) conditions. Heat crossing the boundary surface was that associated with advecting fluids (i.e., no heat diffusion across the boundaries was considered). Initially the reservoir was depressurized to 3 MPa using all five wells, which lowered the temperature to about 1.35 C and produced gas saturation in the formation. The lack of heat diffusion from the boundaries prevented the initial depressurization from continually producing hydrate through dissociation. All simulations reported below were executed with the equilibrium implementation of STOMP-HYD. The equilibrium implementation is equivalent to the kinetic implementation with a high hydrate molecular exchange coefficient. Slow exchange kinetics will increase the concentrations of CO_2 in the mobile phases, yielding earlier breakthroughs with less CH_4 production. The kinetic implementation is currently under development. Simulation results using the kinetic implementation will be reported with the presentation of this paper.

During the production simulations, pure CO_2 was injected into the hydrate-bearing formation through the boundary surfaces that represented the center injection well. The production wells were modeled as constant pressure boundary surfaces, which were maintained at 3 MPa. At the injection wells CO_2 was either injected as gaseous or liquid CO_2, depending on the injection conditions. Simulations were conducted with injection temperatures of 15 and 55 C and injection pressures of 4, 5, and 6 MPa. At 15 C the saturation pressure of CO_2 is approximately 5.07 MPa, which makes the injectant a gas at pressures of 4 and 5 MPa and a liquid at 6 MPa. The injection temperature of 55 C is above the critical point for CO_2 which is at 30.9782 C, making the injectant a supercritical gas. Simulation results in terms of the effluent CO_2 gas concentration, injected mass of CO_2, and produced mass of CH_4 are shown in Figure 1 for injection temperatures of 15 C. Production of the hydrate system was considered to be completed when the concentration of CO_2 in the gas effluent reached a mass fraction of 0.1.

The simulation results show that increasing the injection pressure increases the production rate and decreases the breakthrough time, but does not significantly alter the total produced quantity of methane (Fig. 1). At an injection pressure of 4 MPa, CO_2 breakthrough occurs at 1.05 yr, having injected 473.1 tonne of CO_2 gas, and producing 176.5 tonne of CH_4, which represents 63.6% of the initial CH_4 in the system. At an injection pressure of 5 MPa, CO_2 breakthrough occurs earlier, at 0.546 yr, with 564.8 tonne of CO_2 gas being injected and 171.2 tonne of CH_4 produced (61.8% of the initial quantity). At an injection pressure of 6 MPa, CO_2 breakthrough occurs somewhat earlier, at 0.432 yr, having injected 649.5 tonne of liquid CO_2, and producing 164.0 tonne of CH_4 (59.2% of the initial quantity). Liquid CO_2 forms near the injection well for both the 5 and 6 MPa injections. Elevating the injection temperature to 55 C at 4 MPa has little impact on the CO_2 breakthrough, total injected CO_2 and produced CH_4. The elevated injection temperature does alter the hydrate distribution, however, causing greater hydrate dissociation around the injection well resulting in the formation of secondary hydrate elsewhere in the domain. To illustrate the field conditions during the gas hydrate production color-scaled images of profiles of pressure, MPa; temperature, C; hydrate saturation; gas saturation; liquid-CO_2 saturation; and hydrate mass fraction of CO_2 are shown in Fig. 2 for the injection of liquid CO_2 at 15 C and 6 MPa prior to CO_2 breakthrough at the production wells. Note that Fig. 2 shows one quarter of the five-spot well system, with the injection well located in the lower left-hand corner and the production well in the upper right-hand corner.

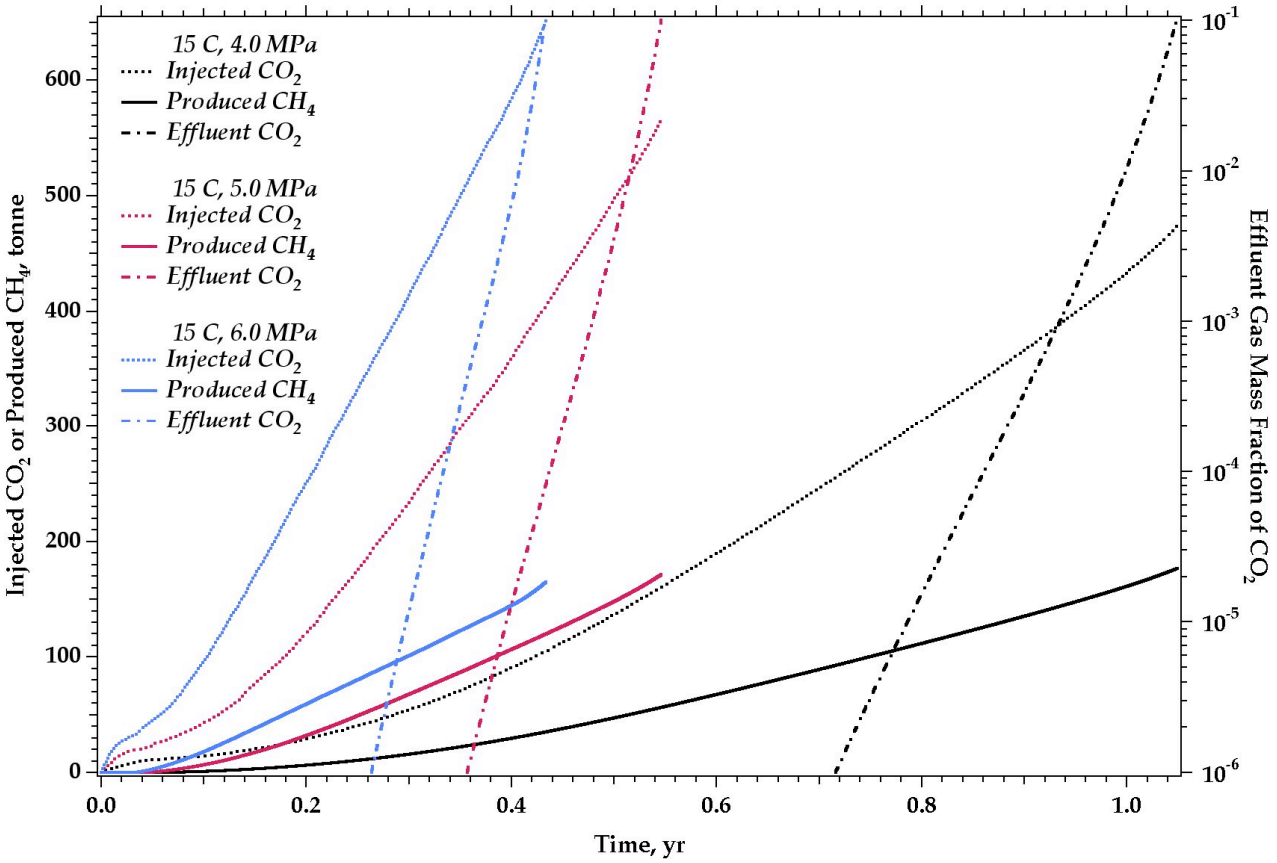

Fig. 1—Methane production rates increase with increasing injection pressure, but total methane produced is nearly invariant with injection pressure.

Discussion

Vast quantities of natural gas are held in hydrate form in geologic reservoirs in sub-oceanic sediments and arctic permafrost zones (Kvenvolden, 1988; Sloan, 1998) where conditions of high pressure and low temperature are within the hydrate stability region. In 1995, the U.S. Geological Survey (USGS) conducted a study to assess the quantity of natural gas hydrate resources in the United States and found that the estimated quantity exceeded known conventional domestic gas resources (Collett, 2004). Recovery of natural gas from these hydrate-bearing deposits has the potential for being economically viable (Circone et al., 2005; Collett, 2004; and Moridis et al., 2004.), but there remain significant technical challenges in converting these natural deposits into a useable resource (Collett, 2004). In conventional reservoirs, natural gas migrates to the recovery point via pressure gradients. For these reservoirs, the recovery rate is a function of the formation permeability and pressure gradients between the reservoir and recovery point. Natural gas recovery from hydrate-bearing deposits requires the additional energetic cost of dissociating the hydrate structure. A variety of methods have been proposed for producing natural gas from hydrate deposits: 1) thermal stimulation, where the temperature is increased above the hydrate stability region; 2) depressurization, where the pressure is decreased below the hydrate stability region; 3) chemical injection of

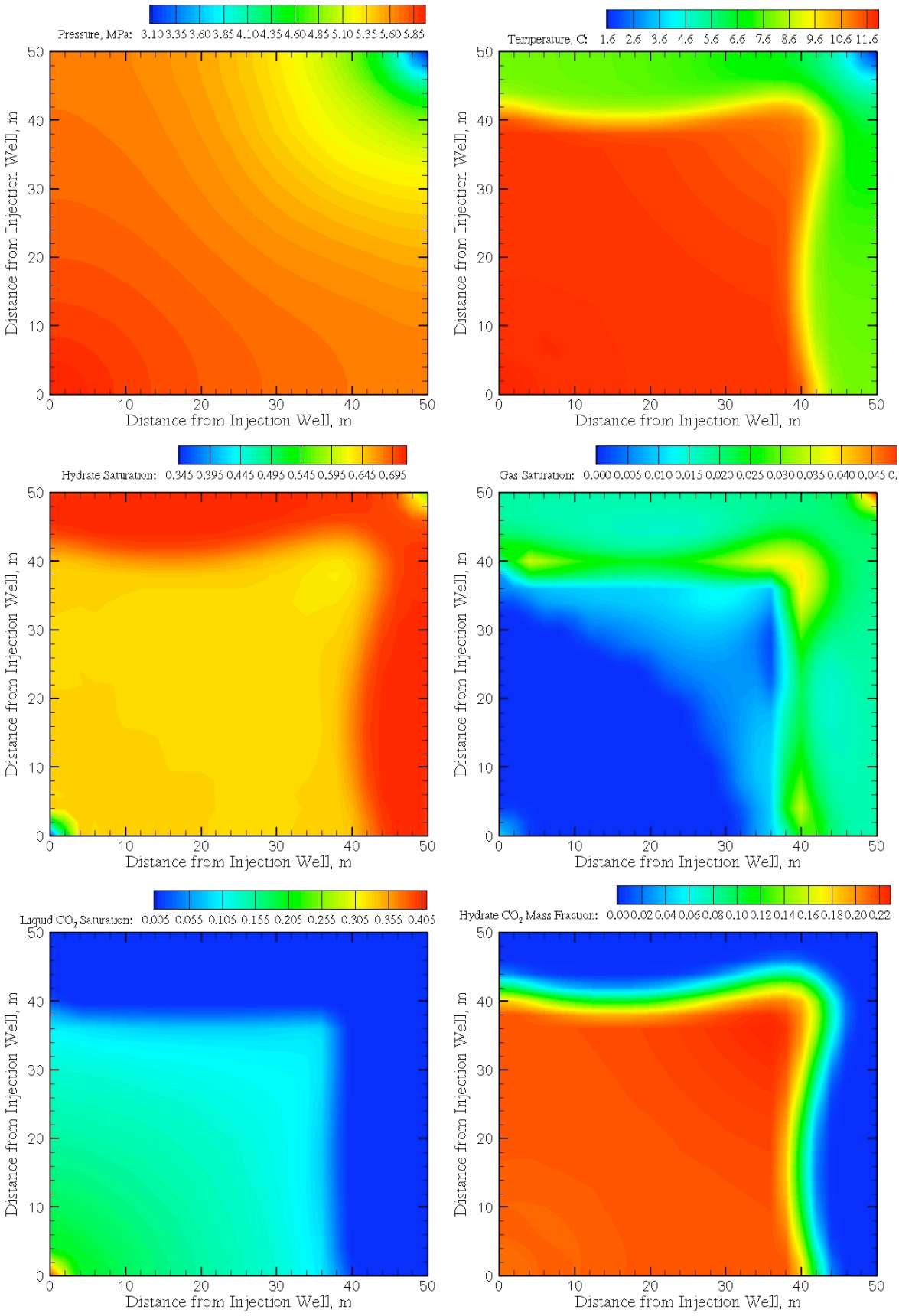

Fig. 2—Field conditions for injection of liquid CO_2 at 15 C and 6 MPa prior to CO_2 breakthrough at the production wells.

inhibitors, where the temperature and pressure conditions for hydrate stability are shifted; and 4) CO_2 or mixed CO_2 and N_2 exchange, where CO_2 and/or N_2 replace CH_4 in the hydrate structure. It is critical to note that although recent estimates (Milkov et al., 2003) put the global accumulations of natural gas hydrate at 3,000 to 5,000 trillion cubic meters (TCM), compared to 440 TCM estimated (Collett, 2004) for conventional natural gas accumulations, that none have speculated how much gas could be produced from these vast natural gas hydrate deposits. What is needed to convert these gas-hydrate accumulations to energy resources are technological innovations, sparked through sustained scientific research and development. As with other unconventional energy resources, the challenge is to first understand the resource, its coupled thermodynamic and transport properties, and then to address its production challenges.

A critical consideration for the production of gas hydrates is the thermal self-regulation of hydrate dissociation. If the hydrate-bearing reservoir is above the freezing point of the formation water, then the temperature in the vicinity of dissociation will decrease because heat flow into the region is insufficient to offset the endothermic heat of dissociation. With continued dissociation, the temperature will decrease until the hydrate is exhausted or the temperature reaches a phase boundary. In the absence of other heat sources (e.g., advective, electromagnetic), the system becomes thermally self-regulating, the temperature remains constant, and the dissociation rate is controlled by diffusive heat transfer. For pressures above the quadruple point (the intersection of the hydrate stability boundary and the formation water freezing point temperature), the lower temperature limit will be that of the hydrate equilibrium boundary. For lower pressures, temperature is limited by the freezing point of the formation water. Laboratory experiments (Circone et al., 2005) have shown that under these conditions, dissociation rates are not slowed by ice formation and are dependent on heat flow into the dissociation zone from the surroundings, and the exothermic heat of formation of the ice contributes to the heat flow into the dissociation area. When the hydrate-bearing formation is below the freezing point of the formation water, however, the dissociation rates are considerably slower (Circone et al., 2005).

Conclusions

Geologic accumulations of natural gas hydrates hold vast organic carbon reserves, which have the potential of meeting global energy needs for decades. Estimates of vast amounts of global natural gas hydrate deposits make them an attractive unconventional energy resource. As with other unconventional energy resources, the challenge is to economically produce the natural gas fuel. Through numerical simulation, this paper has demonstrated the production of geologic accumulations of natural gas hydrates using the CO_2 exchange process with moderate changes in hydrate saturation. Whereas exchanging CO_2 with CH_4 as the guest molecule in gas hydrate is thermodynamically favorable, there are two technical challenges in using this technology for producing geologic deposits: 1) understanding the exchange kinetics and 2) preventing pore plugging through the production of secondary hydrate. To numerically simulate the production process two implementations of a multi-fluid subsurface flow and transport simulator were developed for solving mixed CH_4 and CO_2 hydrate systems in geologic environments; 1) equilibrium, and 2) kinetic. The equilibrium implementation of the simulator assumes thermodynamic equilibrium between the CH_4 and CO_2 components in the mobile (i.e., aqueous, gas, and liquid-CO_2) phases and immobile phases (i.e., hydrate). The second immobile phase, ice, is assumed to have negligible concentrations of CH_4 and CO_2. Both implementations of the simulator solve nonlinear governing equations that describe the conservation of energy and component mass (i.e., H_2O, CH_4, CO_2, and salt) over mobile (i.e., aqueous, gas, liquid-CO_2) and immobile (i.e., hydrate, ice, geologic media, precipitated salt) phases using the integral finite difference approach on structured orthogonal grids. Nonlinearities in the equations are resolved using Newton-Raphson iteration and phase transitions are addressed through primary variable switching.

The gas hydrate challenge is principally technical. Meeting that challenge will require innovation, but more importantly, scientific research to understand the resource and its characteristics in porous media. Producing natural gas from gas hydrate deposits requires releasing methane from its clathrated form. The conventional way to release methane is to dissociate the hydrate by changing the pressure and temperature conditions to those outside of the hydrate stability region. The thermal stimulation production technology effectively dissociates the gas hydrate through heating. Whether the heat source is injected steam, an exothermic reaction, or electromagnetic, the effect is to raise the temperature of the gas hydrate above the equilibrium point, causing the hydrate to dissociate. This approach, however, suffers from poor recovery efficiencies and could possibly disrupt the hydraulic and mechanical properties of the produced reservoir. The depressurization production technology dissociates gas hydrate by lowering the pressure below the hydrate stability point. The self-regulating thermal nature of gas hydrates results in lower temperatures in the dissociation region and ultimately, without an additional heat source, production rates will depend on heat transport into the reservoir (e.g., geothermal gradient). Depressurization is the most economical approach, but could also disrupt the produced reservoir. The inhibitor injection technology causes hydrate dissociation by shifting the equilibrium curve, but the approach is unattractive for environmental and economic reasons. The gas exchange technology releases methane by replacing it with a more thermodynamic molecule (e.g., carbon dioxide, nitrogen). This technology has three advantageous: 1) it sequesters greenhouse gas, 2) it releases energy via an exothermic reaction, and 3) it retains the hydraulic and mechanical stability of the hydrate reservoir. This technology currently has one disadvantage; its novelty. The gas exchange technology currently appears promising, but its success or failure will depend on the results of future scientific research and associated technological innovations.

References

Booth, J.S., Rowe, M.M., Fischer, K.M. 1996. Offshore gas hydrate sample database with an overview and preliminary analysis. U.S. Geological Survey, Open File Report 96-272, Denver, Colorado.

Castaldi, M.J., Y. Zhou, and T.M. Yegulalp. 2007. Down-hole combustion method for gas production from methane hydrates. *Journal of Petroleum Science and Engineering*, 56:176-185.

Circone, S., S.H. Kirby, and L.A. Stern. 2005. Thermal regulation of methane hydrate dissociation: Implications for gas production models. *Energy & Fuels*, 19(6):2357-2363.

Collett, T.S. 2004. Gas hydrates as a future energy resource. *Geotimes*, 49(11):24-27.

Englezos, P. 1993. Clathrate hydrates. *Ind. Eng. Chem. Res.*, Vol. 32: 1251-1274.

Hirohama, S., Y. Shimoyama, A. Wakabayashi, S. Tatsuta, and N. Nishida. 1996. Conversion of CH_4-hydrate to CO_2-hydrate in liquid CO_2. *Journal of Chemical Engineering of Japan*, 29(6):1014-1020.

Kvenvolden, K.A. 1988. Methane hydrate - a major reservoir of carbon in the shallow geosphere? *Chemical Geology*, 71:41-51.

Klauda, J.B., and S.I. Sandler. 2003. Phase behavior of clathrate hydrates: a model for single and multiple gas component hydrates. *Chemical Engineering Science*, 58:27-41.

Komai, T.; Yamamoto, Y.; and Ikegami, S. 1997. Equilibrium properties and kinetics of methane and carbon dioxide gas hydrate formation/dissociation. *Proceedings of American Chemical Society Fuel Chemistry Division*, 42(2):568-572.

McCabe, W.L., J.C. Smith and P. Harriot. 2005. *Unit Operations of Chemical Engineering* (seventh ed.), New York: McGraw-Hill, pp. 163-165, ISBN 0-07-284823-5.

McGrail, B.P., T. Zhu, R.B. Hunter, M.D. White, S.L. Patil, and A.S. Kulkarni. 2004. A new method for enhanced production of gas hydrates with CO2. *Gas Hydrates: Energy Resource Potential and Associated Geologic Hazards*, American Association of Petroleum Geologists.

Milkov, A.V., G.E. Claypool, Y.J. Lee, W.Y. Xu, G.R. Dickens, and W.S. Borowski. 2003. In situ methane concentrations, at Hydrate Ridge, offshore Oregon: New constraints on the global gas hydrate inventory from an active margin. *Geology*, 31(10):833-836.

Moridis, G.J., T.S. Collett, S.R. Dallimore, T. Satoh, S. Hancock, and B. Weatherill. 2004. Numerical studies of gas production from several CH4 hydrate zones at the Mallik site, Mackenzie Delta, Canada. *Journal of Petroleum Science and Engineering*, 43(3-4):219-238.

Mualem, Y. 1976. A new model for predicting the hydraulic conductivity of unsaturated porous media. *Water Resources Research*, 12:513-522.

Nakano, S., K. Yamamoto, and K. Ohgaki. 1998. Natural gas exploitation by carbon dioxide from gas hydrate fields - High-pressure phase equilibrium for an ethane hydrate system. *Proceedings of the Institution of Mechanical Engineers*, Vol. 212:159-163.

Ohgaki, K., K. Takano, H. Sangawa, T. Matsubara, and S. Nakano. 1996. Methane exploitation by carbon dioxide from gas hydrates – Phase equilibria for CO2-CH4 mixed hydrate system. *Journal of Chemical Engineering of Japan*, Vol. 29(3):478-483.

Østergaard, K.K., R. Masoudi, B. Tohidi, A. Danesh, and A.C. Todd. 2005. A general correlation for predicting the suppression of hydrate dissociation temperature in the presence of thermodynamic inhibitors. *Journal of Petroleum Science and Engineering*, Volume 48(1-2):70-80.

Rice, W. 2003. Proposed system for hydrogen production from methane hydrate with sequestering of carbon dioxide hydrate. *Journal of Energy Resource Technology* (ASME), 125(4):253–256.

Rice, W. 2006. Hydrogen production from methane hydrate with sequestering of carbon dioxide. *International Journal of Hydrogen Energy*, 31(14):1955-1963.

Setzmann, U., and W. Wagner. 1991. A new equation of state and tables of thermodynamic properties for methane covering the range from the melting line to 625 K at pressures up to 1000 MPa. *J. Phys. Chem. Ref. Data*, 20(6):1061-1155.

Sloan, E.D., Jr. 1998. *Clathrate Hydrates of Natural Gases*, 2nd ed., Marcel Dekker, Inc., New York.

Smith, D.H., K. Seshadri, and J.W. Wilder. 2001. Assessing the thermodynamic feasibility of the conversion of methane hydrate into carbon dioxide hydrate in porous media. *Proceedings of First National Conference on Carbon Sequestration*, National Energy Technology Laboratory.

Span, R. and W. Wagner. 1996. A new equation of state for carbon dioxide covering the fluid region from the triple-point to 1100 K at pressures up to 800 MPa. *J. Phys. Chem. Ref. Data*, 25(6):1509-1588.

U.S. Environmental Protection Agency. 2006. The significance of methane and activities to reduce methane emissions, *Methane to Markets Bulletin*, www.methanetomarkets.org.

van Genuchten, M.T.A. 1980. A closed-form equation for predicting the hydraulic conductivity of unsaturated soils. *Soil Sci. Soc. Am. J.*, 44:892-898.

White, M.D., and M. Oostrom. 2000. *STOMP Subsurface Transport Over Multiple Phases, Version 2.0, Theory Guide*, PNNL-12030, UC-2010, Pacific Northwest National Laboratory, Richland, Washington.

White, M.D. and B.P. McGrail. 2006. STOMP-HYD: A new numerical simulator for analysis of methane hydrate production from geologic formations. *Proceedings of 2nd International Symposium on Gas Hydrate Technology*, 1-2 November 2006, KIGAM, Daejeon, Korea.

Nomenclature

a = carbon dioxide (CO_2) component (superscript)

CH_4 = methane component (superscript)

CO_2 = carbon dioxide component (superscript)

D_γ^i = molecular diffusion coefficient, L^2/t, m^2/s

$\mathbf{D}_{h_\gamma}$ = phase hydraulic dispersion coefficient vector, L^2/t, m^2/s

g = gas phase (subscript)
g = acceleration of gravity, L/t^2, m/s^2
h = hydrate phase (subscript)
h_γ = phase enthalpy, L^2/t^2, J/kg

H_2O = water component (superscript)
i = ice phase (subscript)
i = component indicator (superscript)

$\mathbf{J}_g^i$ = gas diffusive/dispersive component flux vector, m/L^2 t, kg/m^2 s

$\mathbf{k}$ = intrinsic permeability vector, L^2, m^2

$\mathbf{k}_e$ = effective thermal conductivity vector, m L/t^3 T, W/m K

$k_{r\gamma}$ = phase relative permeability

K_h = hydrate molecular exchange rate coefficient, s/m^2, kg/m^3 s Pa

l = aqueous phase (subscript)

m_γ = phase mass source, m/t, kg/s

M^i = component molecular weight, m/n, kg/kmol
M_γ = phase molecular weight, m/n, kg/kmol

n = liquid-CO_2 phase (subscript)
o = methane (CH_4) component (superscript)
p = precipitated salt phase (subscript)

P_g^i = component vapor partial pressure, m/L s^2, Pa

P_h^{eq} = hydrate equilibrium pressure, m/L s^2, Pa

P_n^c = critical liquid CO_2 pressure, m/L s^2, Pa

$P_{sat}^{CO_2}$ = CO_2 saturated vapor pressure

P_γ = phase pressure, m/L s^2, Pa

q = heat source, m L^2/t^3, W

$\overline{\overline{s}}_l$ = apparent aqueous saturation

s_{lr} = residual aqueous saturation

$\overline{\overline{s}}_t$ = apparent total-liquid saturation

s_γ = phase saturation

t = time, t, s
t = total liquid (subscript)
T = temperature, T, K [C]

T_h^{eq} = hydrate equilibrium temperature, T, K [C]

$\mathbf{z}_g$ = gravitation unit vector

u_s = grain internal energy, L^2/t^2, J/kg

u_γ = phase internal energy, L^2/t^2, J/kg

$\mathbf{V}_\gamma$ = phase flux vector, L/t, m/s

w = water (H_2O) component (superscript)

β_{gl} = gas-aqueous scaling factor

β_{gn} = gas-liquid CO_2 scaling factor

β_{nl} = liquid CO_2-aqueous scaling factor

γ = phase indicator (subscript)

μ_γ = phase viscosity, m/L t, Pa s

ρ_γ = phase density, m/L^3, kg/m^3

ρ_s = grain density, m/L^3, kg/m^3

σ_{gl} = gas-aqueous interfacial tension, m/t^2, N/m [dyne/cm]

σ_{gn} = gas-liquid CO_2 interfacial tension, m/t^2, N/m [dyne/cm]

σ_{nl} = liquid CO_2-aqueous interfacial tension, m/t^2, N/m [dyne/cm]

σ_{ref} = reference interfacial tension, m/t^2, N/m [dyne/cm]

φ_g^i = gas mole fraction of hydrate formers

ϕ_D = diffusive porosity

ϕ_T = total porosity

τ_γ = phase tortuosity factor

χ_γ^i = phase mole fraction

ψ = entry pressure m/L s^2, Pa

ω_γ^i = phase mass fraction